Warsaw 2005

MOLECULAR DYNAMICS MODELING FOR ENHANCED INTERPRETATION OF TEM IMAGES

Kurt Scheerschmidt

Max Planck Institute of Microstructure Physics, Weinberg 2, D-06120 Halle, Germany,
schee@mpi-halle.de, http://www.mpi-halle.mpg.de/~md_simul

The imaging of crystal defects by high-resolution transmission electron microscopy (HRTEM) or with the help of electron diffraction contrast techniques (conventional bright- or dark-field TEM) is well known and routinely used. Although the theoretical image calculations always tend to establish standard rules of interpretation, a direct and phenomenological analysis of electron micrographs is mostly not possible, thus requiring the application of image simulation and matching techniques [1]. Images are modeled by calculating both the interaction process of the electron beam with the almost periodic potential of the matter, and the subsequent Fourier imaging process including the microscope aberrations. The simulations are fitted to the experiment by varying the defect model and the free parameters. This trial-and-error image matching technique is the indirect solution to the direct scattering problem applied to analyze the defect nature under investigation (e.g. [2]).

Two topics for an enhanced interpretation of TEM and HREM will be discussed in detail: Modeling the atomic structure of the objects based on molecular dynamics and possibilities to overcome the trial-and-error image matching using direct methods.

1. Molecular dynamics structure modeling

The ability of modern computing allows one to predict materials properties by using quantum-theoretical ab initio calculations with a minimum of free parameters, which, however, are very restricted to small structures only, even with suitable linearization and tight-binding based approximations. Thus the classical molecular dynamics (MD) method using suitably fitted many-body empirical potentials have to be applied to simulate atomic processes with macroscopic relevance. Such simulations enable a sufficiently large number of particles and relaxation times up to μs to be considered. However, in the empirical MD the electronic structure and the nature of the covalent bonds can only be described indirectly.

Empirical MD solves Newton's equations of motion for a system of particles yielding all their trajectories by using constant volume or pressure (NVE or NpT ensemble), and time steps of the order of 0.25 fs to ensure the proper calculation of surface modes. NVE is preferred for free surfaces and simulations to calculate diffusion processes, whereas NpT enables the relaxation of the cell dimensions and the application of an outer pressure. Energy dissipation out of the models or temperature gradients are controlled by rescaling the velocities of atoms in the outer layers only (cf. Fig.1). In addition, for straight defects created at interfaces the system is dynamically coupled to an elastic continuum using an extended Lagrangian formalism. Simple force-field potentials are restricted in their validity to small deviations from the equilibrium. A better potential most often used for semiconductors is the Stillinger-Weber (SW) potential, including 3-body next neighbour interactions [3], which allows rescaling to avoid preordering of surfaces. The potential of Tersoff [4] with different parametrizations (Si, Ge, hydrogenated Si, Si-SiC, etc.) has the shape of a bond order, which is a completely different functionality. The bonds are weighted by the bond order including all many body interactions over neighbours different from the actual bonding pair. Compared to each other [5], the empirical potentials offer advantages and disadvantages in range of

validity, physical meaning, fitting and accuracy as well as applicability. Such restrictions exist for other potential types, too, e.g. the (modified) embedded atom approximation (MEAM, [6]), and no potential is applicable for long range interactions. In addition, the inter-atomic forces in covalent solids can only be completely described if the influence of the local environment according to the electronic structure is included. Therefore, the fit of the empirical potentials has to be supported by ab initio calculations and, in addition, it is of importance to find physically motivated semi-empirical potentials starting from analysis of the band energy mostly with the moments of the electron density and using tight-binding (TB) representations [7]. The repulsive energy is assumed to be an embedded pair interaction, the promotion energy reflects the energy difference of valence s and p electrons. The band energy is the expansion of the electronic energy into hopping matrix elements and bond order terms. A second moment approximation (BOP2) of the tight-binding model can be used to establish a general form at the level of the Tersoff potential with at least only four free fit parameters [8]. A further enhancement is based on BOP4, which is given up to the fourth-level continued fraction of the Greens function and necessary to describe correctly the π-bonds [9].

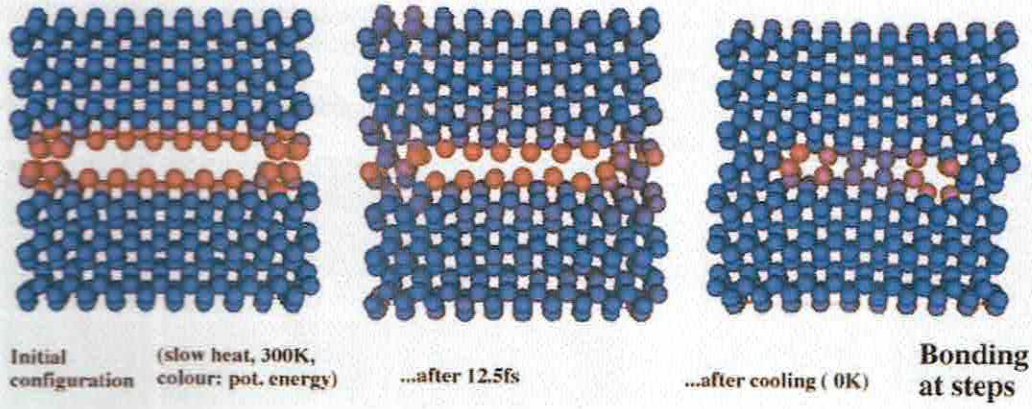

Fig. 1: Energy dissipation during bonding at steps (slow heat transfer, red colour indicating higher potential energy above ground state, which is blue)

Different applications are treated successfully, e.g. predicting structure of and defects at wafer bonded interfaces, relaxation of quantum dots and wells, diffusion and precipitation of silver in glasses, hydrogenisation of surfaces etc. In the present paper mainly the results are discussed which are related directly to an enhanced TEM interpretation. Fig.2 shows experimental HREM of 60° dislocations due to bonding over steps and simulated images using the model of Fig.1. The analysis of the structural details of various relaxed interacting Si(001) surfaces have shown that special structural units may occur [10], in particular for 90° twist rotation the interface results in the so called "dreidl" structure (cf. Fig. 3). DFT calculations revealed the stability and relative energy minima of these units. The differences in the band structure compared to perfect bulk Si may offer bandgap tailoring by controlling the structure of bonded interfaces. Applying a small twist rotational misorientation results in a mosaic-like bonded interface structure [11]. After bonding and sufficient relaxation under slow heat transfer conditions, almost all atoms have a bulk-like environment separated by misfit screw dislocations, which may have a high rate of kinks and form a network. Similarly, a prescribed network of two sets of a/2[110] screw dislocations, which accommodate a small rotationally twist, is relaxing into a configuration by breaking symmetry. Fig.4 shows typical plan view experimental and simulated TEM contrast of such screw networks. MD simulations as well as TEM and HREM investigations showed further [10] that the screw dislocations forming the network of the (001) low-angle twist grain boundary can dissociate intrinsically into two 30° partials along the {111} glide plane (cf. Fig.5).

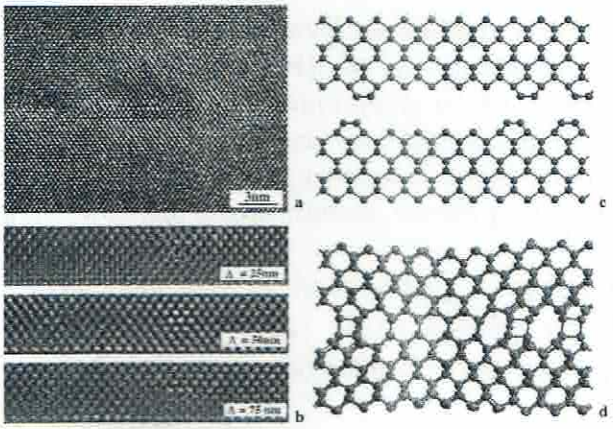

Fig.2: Cross-sectional 200kV HREM image of the interface of two (100) silicon wafer bonded in UHV at room temperature, (b) Simulated images (defoci in nm) of molecular dynamics generated structures describing bonded wafers with an initial rotational misfit of 4.58°, (c) Starting configuration and (d) Snapshot at 1ps of molecular dynamics for waferbonding at Si (100) surfaces with atomic-height steps.

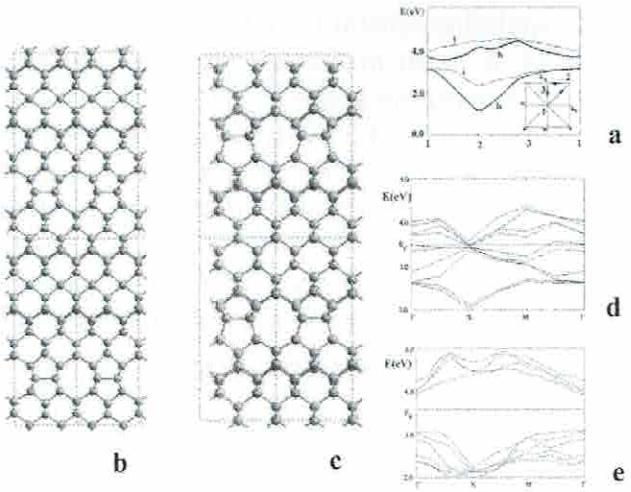

Fig.3: (a) DFT-LDA band structure of the dreidl interface (bands i,) versus a bulk silicon crystal (bands b), (b,d) [110]-projection of the bonded Pmm(m) interface and DFT-LDA band structure, (c,e) [110]-projection of the bonded P(4)m2 interface (dreidl structure) and DFT-LDA band structure (enlarged gap regions are shown).

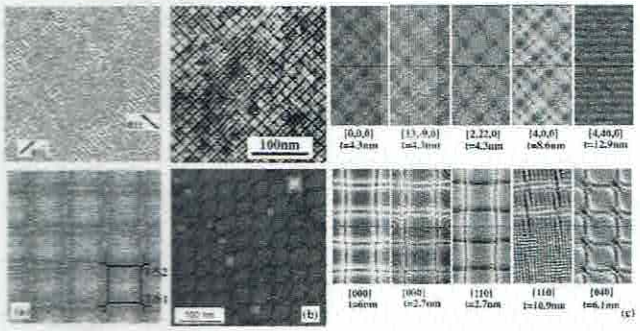

Fig. 4: Rotationally misoriented waferbonding: (a) Metastable kinked screw dislocation network of 4.6° rotated wafers after 2.5ps SW-MD relaxation at 900K, (b) D=10b screw lattice (b=a/2<110>) showing two different nodes T1, T2, (c) Experimental plan view images of screw dislocation networks of UHV-bonded (100) Si interfaces with different sample thicknesses and orientations (courtesy R. Scholz, MPI Halle), (d) Simulated plan view TEM images for different thicknesses t and beam orientations indicated by the [hkl]-pole excitation (upper/lower row correspond to model a/b).

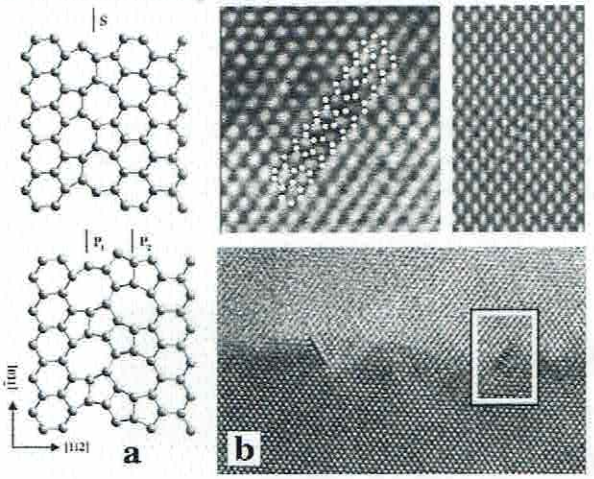

Fig. 5: Defect core reconstructions: (a)[111] projections of the perfect 1/2[110] screw dislocation (S) and the dissociated 30° partials (P) after 3-step MD relaxation, (b) [110] cross sectional HREM image of a waferbonded twist boundary: stacking fault ribbon bounded by two 30° partials, and image simulation from a MD relaxed model.

2. Possibilities of direct object retrieval

Electron holography [12] or other reconstruction techniques [13] permit the determination of the scattered exit wave function directly out of the hologram or from defocus series up to the microscope information limit. Especially the sidebands of a Fourier-transformed hologram represent the Fourier spectrum of the complete complex image wave and its conjugate, respectively, from which the object wave can be reconstructed by separating, centring, and applying the inverse Fourier transform (cf. the retrieval scheme in Fig. 6 applied to determine thickness and object bending locally). Using reconstructed exit waves, the trial-and-error iterative image matching can be replaced by

direct object data retrieval via suitably linearized and regularized analytical inverse solutions of the scattering problem [14]. Inverse problems are fascinating but difficult and in most of the cases mathematically ill or improperly posed. However, the direct retrieval of object information as, e.g., the local object thickness and orientation, by solving the inverse scattering problem, enables a reliable enhancement of quantitative image interpretation of electron micrographs, and is the basis of a general object reconstruction, mostly providing a better insight into the basic relations of the physical phenomena.

The main steps of the retrieving procedure with respect to the local sample thickness and orientation are as follows (cf. Fig.6): Starting, e.g., from a hologram all reflections are separately reconstructed yielding the moduli and phases of the plane waves at the exit surface Φ^{exp}.

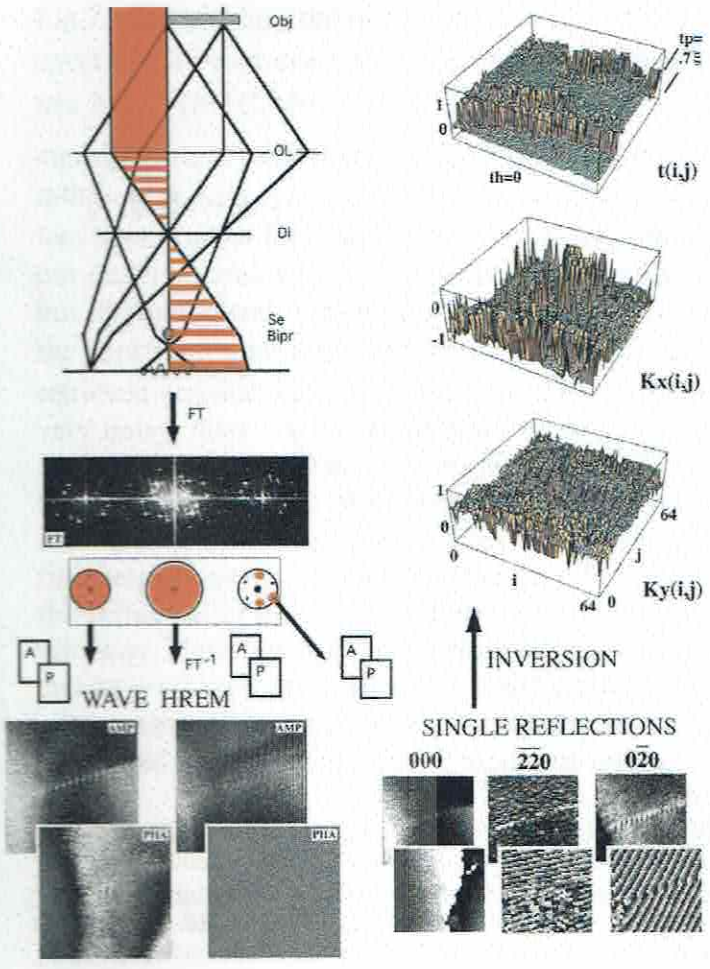

Fig. 6: Wave reconstruction using electron holography and object retrieval (thickness t and beam orientation K_{xy} schematic and determined for an Au twist boundary).

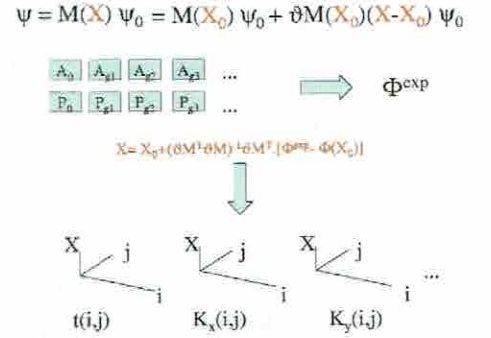

Fig. 7: Matrix formulation of the dynamical theory as the basis of local linearization and inversion: The moduli and phases of the exit wave are the input to the generalized inverse yielding thickness and orientation as function of the position in the pixel space.

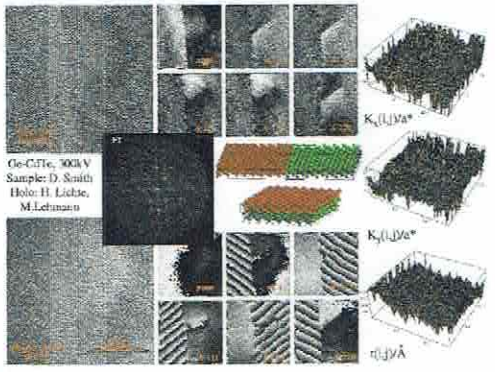

Fig. 8: Object retrieval (thickness t and beam orientation K_{xy}) at an Ge-CdTe interface (moduli/phases of reconstructed single reflections in upper/lower rows, insets: sideband of Fourier transformed hologram and structure models used for exit wave calculations).

Then the Bloch waves are calculated for an a priori diffraction geometry, i.e., a scattering model characterized by the number of beams and the scattering potential, and by assuming a suitable trial average beam orientation (K_{xo}, K_{yo}) predetermined by the experiment. With the sample thickness t_o as a free parameter, the perturbation approximation (cf. Fig. 7) yields both the moduli and the phases of the plane wave amplitudes as linear functions of the object thickness t and orientation (K_x,K_y). The comparison of the theoretical amplitudes and phases with the experimental ones for each reflection and at each image pixel yields a linear equation system for the sample thickness, beam orientation etc. The analytic form of the equations enable the inverse solution as given in Fig.7, thus yielding the local thickness t_{ij} and bending $(K_x,K_y)_{ij}$ of the object with respect to the beam orientation for each image pixel (i,j). Here, however, the inverse matrix $M_{inv}=(M^T C_1 M+\gamma C_2)^{-1} M^T$ has to be a generalized and regularized one, which is equivalent to a maximum-likelihood solution or a least-square minimization of $\|\Phi^{exp}-\Phi^{th}\|+\gamma\|\Omega\|=Min$. The reason for this difficulty is the ill-posedness of the inverse problem based on the fact that the problem is over-determined with respect to the unknowns but underdetermined if the noise is included. The resulting solution is now well-posed but ill-conditioned, which may be controlled and optimized by pixel smoothing via C_1, the constraint matrix C_2, and the regularization parameter γ in M_{inv}. Nevertheless, the retrieved non-stabilized solution from the experimental hologram of a grain boundary is very noisy, there are distinct regions of thickness for the hole and the plateau of the reconstruction in Fig. 6 and the retrieval of the Ge-CdTe interface in Fig. 8 showing the thickness step and the object bending along the grain boundary. The interface region in the experimental examples itself occurs as a modeling error. Smoothing the data or the first derivatives and regularizing the generalized inverse solution may drastically reduce the influence of noise and outliers. The ambiguities, however, cannot be corrected in this way. Here much more a priori information is necessary to avoid modeling errors and to overcome the difficulties resulting from missing data. The applicability of the object retrieval demands the knowledge of the confidence region, the conditions for stability, and the restrictions due to modeling errors.

[1] D. B. Carter, C. B. Carter, TEM-A Textbook for Materials Science, Plenum Press, N.Y., 1996
[2] G. Möbus, et al., J. Microscopy **190** (1998) 190, D. van Dyck, *J. Microscopy* **190** (1998) 190
[3] F.H. Stillinger, T.A. Weber, *Phys. Rev. B* **31** (1985) 5262
[4] J. Tersoff, *Phys. Rev. B* **38** (1989) 9902 & *Phys. Rev B* **39** (1989) 5566
[5] S. Balamane, T. Halicioglu, W.A. Tiller, *Phys. Rev. B* **46** (1992) 2250
[6] M.I. Baskes, *Phys. Rev. B* 46 (1992) 2727
[7] D. G. Pettifor, I.I. Oleinik, *Phys. Rev. B* **59** (1999) 8487
[8] D. Conrad, K. Scheerschmidt, *Phys. Rev.B* **58** (1998) 4538
[9] D. Conrad, K. Scheerschmidt, U. Gösele, *Appl. Phys. Lett.* **77** (2000) 49
[10] K. Scheerschmidt, D. Conrad, A. Belov, *Computational Materials Science* **24** (2002)33
[11] A.Y. Belov, R. Scholz, K. Scheerschmidt, *Philos. Mag. Lett.* **79** (1999) 531 & K. Scheerschmidt, V. Kuhlmann, *Interface Science* **12** (2004) 157
[12] H. Lichte, *Advances in Optical and Electron Microscopy* **12** (1991) 25 & M. Lehmann, H. Lichte, *Microsc. Microanal.* **8** (2002) 447
[13] A. Thust, et al., *Ultramicroscopy* **64** (1996) 211
[14] K. Scheerschmidt, *Lecture Notes in Physics* **486** (1997) 71 & *J. Microscopy* **190** (1998) 238